Supporting Information: SLPcalculator: a web-based tool to estimate nanoparticle heating with peak analysis and F-test.

Iago López-Vázquez,[a,b] Yilian Fernández-Afonso,[c,d] Antonio Santana-Otero,[a] Sergiu Ruta,[e] Alfredo Amigo,[a] M. Puerto Morales,[d] Roy W Chantrell,[f] Lucía Gutiérrez,[c] David Serantes,[a,b]

1 Illustration of Type B uncertainty sources

In order to illustrate the origin and evaluation of the Type B uncertainties discussed in the main text, Fig. 1 shows two representative examples. Panel (a) demonstrates how the ambiguity in defining the exact peak temperature arises from the presence of a short plateau of nearly identical values, from which the FirstMax and LastMax points are used to estimate the corresponding spread in the calculated SLP values. Panel (b) shows a representative case where a change in concavity may obscure the definition of the true starting point of the heating curve, highlighting the uncertainty that would appear in the ISM approach.

2 RMSE as an intuitive complement to the F-test

To give a more intuitive idea of how the F-test identifies the linear range, in the following we present the root mean square errors (RMSE) of the linear and quadratic fits and highlighted the regions where the F-test supports the simpler (linear) model. The RMSE is defined as:

$$\mathrm{RMSE}(x) = \sqrt{\frac{\sum_{i=1}^{n}(y_i - y_{\mathrm{fit}})^2}{N-m}}, \qquad (1)$$

where y_i are the experimental data points, and y_{fit} are the corresponding fitted values. In Fig.2 we present RMSE as a function of time (and of the number of points) considered for both linear and quadratic fits.

As stated before, Figures 2 (a) and (b) correspond, respectively, to the RMSE fits performed in the cooling branch of the $\Delta T(t)$ curve, starting from the peak, for the PAM analysis, and in the initial heating branch, which is employed in the ISM method.According to the F-test, the heating region to the left of the peak, from where we obtain the heating slope in the PAM, can be considered linear over a relatively wide time range (10-15 seconds). This indicates that, when applying the PAM, the extent of the linear regime is mainly determined by the cooling branch after the peak, rather than by the last points of the heating stage. Consequently, in the case of PAM, we determined the linear range from the cooling branch, since the heating branch can usually be safely assumed to exhibit linear behavior regardless of the number of points or the time interval considered, as verified with the F-test. This time window was then used consistently to compute both the heating and the cooling slopes.

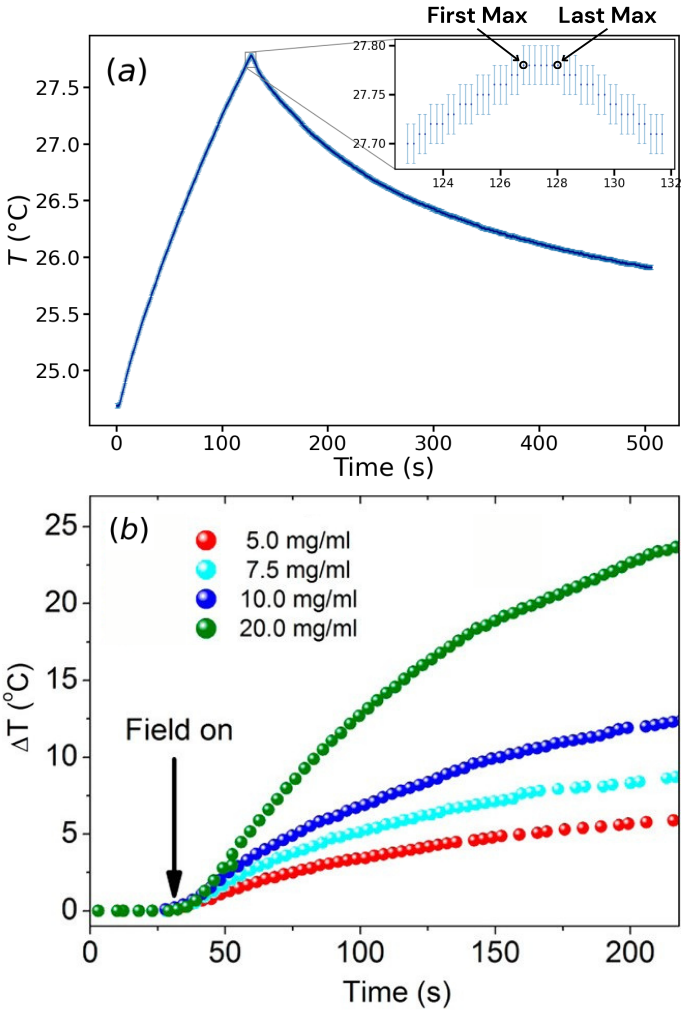

Fig. 1 (a)Example of the procedure used to define the Type B uncertainty associated with the peak temperature. The inset highlights the region around the maximum of the ΔT(t) curve, where a plateau of several points with nearly identical values is observed. The first (FirstMax) and last (LastMax) points within this plateau are taken to compute the corresponding spread in the calculated S, which is then used to define the Type B contribution to the uncertainty.(b) Representative experimental heating curves illustrating how the concavity change may hinder the identification of the true starting point of the temperature rise ("time zero"). Figure adapted from [1].

As observed in Figures 2 (a) and (b), the region defined by the the F-value falling below the critical threshold accurately identi-

[a] Applied Physics Department, Universidade de Santiago de Compostela, Spain
[b] Instituto de Materiais (iMATUS), Universidade de Santiago de Compostela, Spain.
[c] Instituto de Nanociencia y Materiales de Aragón (INMA, UNIZAR-CSIC)
[d] Instituto de Ciencia de Materiales de Madrid (ICMM-CSIC)
[e] College of Business, Technology and Engineering, Sheffield Hallam University, UK.
[f] School of Physics, Electronics and Technology, The University of York, York, UK

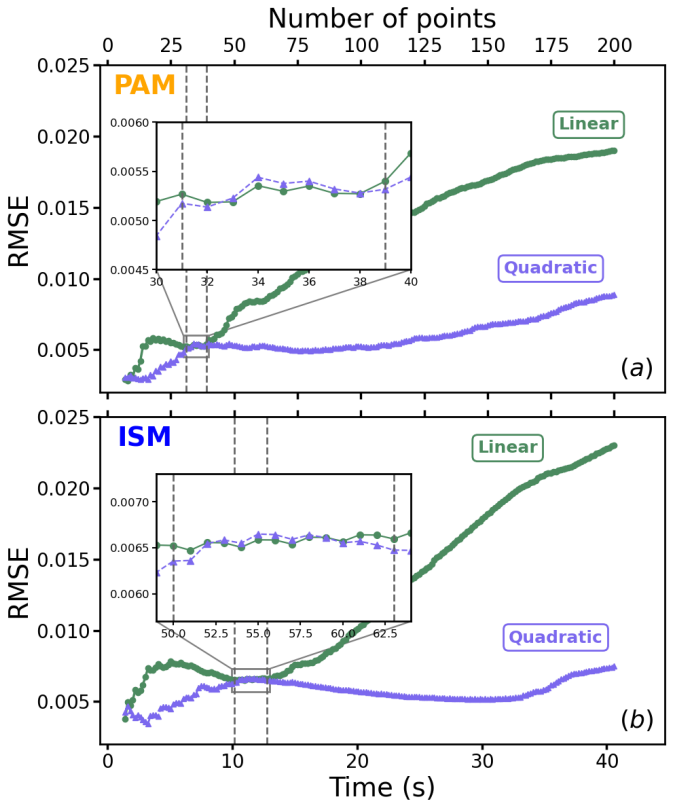

Fig. 2 Root-mean-square error (RMSE) of linear (green) and quadratic (purple) fits as a function of the number of points for both PAM (a) and ISM (b), with the vertical dashed gray lines indicating the intervals where the F-test condition ($F < F_{\text{crit}}$) is satisfied. The insets show the approximate correspondence between the linear range identified by the F-test and the region where the linear fit yields a smaller error than the quadratic one.

fies the time interval within which the quadratic form makes no improvement over the linear fit, as also reflected by the crossover of the RMSE curves, where the linear RMSE becomes smaller than the quadratic one. It should be noted that the RMSE analysis is shown only as a complementary (more intuitive) example only; the F-test is the more robust statistical analysis that allows the identification of the linear range, as it allows the selection of significance levels, which the RMSE alone does not.

3 Initial temperature variations

As discussed in the main text, small variations in the initial temperature may contribute to the observed variability among datasets. Figure 3 shows the raw temperature profiles obtained from the 30 repeated measurements, highlighting the dispersion in both the initial and peak temperatures. Figure 4 summarizes these results by comparing the corresponding initial and peak temperatures for the different heating times.

No systematic trend with the order of acquisition was observed, indicating that the variability arises from random experimental fluctuations rather than from cumulative heating effects. These results illustrate the experimental challenges associated with calorimetric SLP determination and further motivate the use of repeated measurements and statistical averaging.

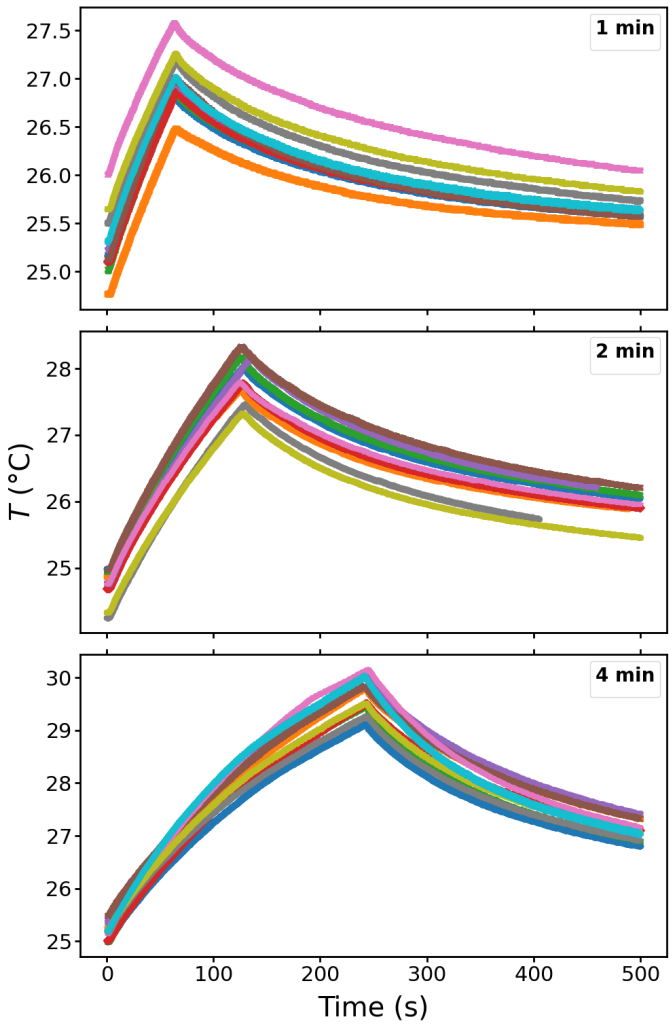

Fig. 3 Temperature profiles obtained in 10 repeated heating experiments performed under identical experimental conditions for three different heating durations (1, 2 and 4 min).

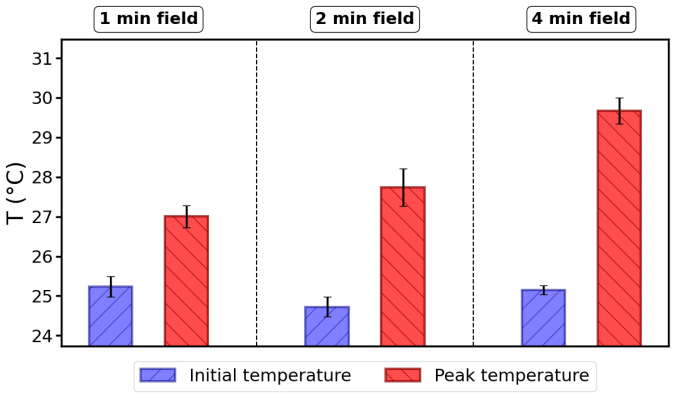

Fig. 4 Comparison between initial and peak temperatures obtained for different heating times under the applied magnetic field. Bars represent the mean values with standard deviation as error bars. Blue hatched columns correspond to the initial temperature, while red hatched columns correspond to the peak temperature.

4 Description of finite-element simulations (COMSOL © Multiphysics)

We solved the transient heat-conduction problem using the *Heat Transfer in Solids* and *Heat Transfer in Fluids* interfaces. The 3D, time-dependent model geometry included the sensor tip (coating) and a short length of fused-silica fiber. All materials were assumed to be isotropic. In the fluids (water and air headspace), the velocity field was set to $\mathbf{u} = \mathbf{0}$, so that transport was diffusion-controlled (that is, no convective flow was allowed).

Governing equation.

$$\rho C_p \frac{\partial T}{\partial t} = \nabla\cdot(k\nabla T) + Q. \tag{2}$$

Materials. Material properties were taken from the *COMSOL Material Library* (v6.1) for water (liquid), air, glass (vial wall) and fused silica (fiber). The coating was modelled as polytetrafluoroethylene (PTFE), with (k,ρ,C_p) evaluated at 25 °C. All properties were treated as temperature-dependent wherever available.
Geometry. The 3D model (Fig. 5) consists of a closed cylindrical glass vial (inner radius R_i, wall thickness $t_w = 0.5$ mm, height H_{vial}) partially filled with water ($V = 1.00$ mL), which gives a liquid height $H_{\text{liq}} = V/(\pi R_i^2)$ ($H_{\text{liq}} = 12.7$ mm for $R_i = 5$ mm). Above the liquid, an air headspace of height $H_{\text{air}} = H_{\text{vial}} - H_{\text{liq}}$ is included. To minimise artificial boundary effects on the temperature field, the vial is embedded in a surrounding cylindrical air domain of radius $5R_i$ and height $5H_{\text{vial}}$. A fiber-optic sensor is placed along the axis; its wetted tip consists of an ETFE coating of thickness d in front of the fused-silica fiber. The reported temperature is the volume average over a microdomain (radius 40 μm, height 50 μm) centred on the axis at a depth d below the coating.

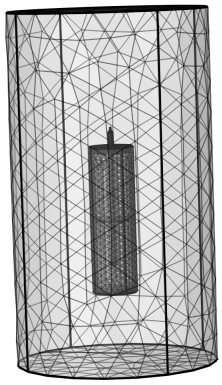

Fig. 5 Finite-element mesh of the 3D model. The outer transparent cylinder corresponds to the surrounding air domain, while the inner cylinder represents the glass vial and liquid sample. The fiber-optic sensor with its coated tip is placed along the axis.

Mesh. An unstructured tetrahedral mesh was used, with strong local refinement in the coating and microdomain (at least 10 elements through the coating thickness; growth factor 1.2–1.3). The total cell count was $\mathcal{O}(10^5$–$10^6)$. Mesh independence was verified.

Boundary and initial conditions. The system was modelled as non-adiabatic, with heat losses to an ambient reservoir held at $T_0 = 25$ °C. Numerically, this was implemented by fixing $T = T_0$ at the outer boundary of the surrounding air cylinder, mimicking a thermostated environment (for example, a cooling bath). The initial temperature field was set to a uniform value $T(\mathbf{x},0) = T_0$.

Solver. A time-dependent BDF scheme was employed, fully coupled with the direct solver PARDISO, with a relative tolerance of 10^{-4}.

Heating term (EMH/photothermal). Electromagnetic hyperthermia / photothermal experiments were modelled as a uniform volumetric heat source in the liquid domain. The power density was taken as $Q = \text{SAR}\,C_{\text{m}}$, where $\text{SAR} = 200$ W g^{-1} is the specific absorption rate and C_{m} is the nanoparticle (iron) mass concentration in g m^{-3}. For a representative suspension with $C_{\text{m}} = 1$ mg mL$^{-1} = 1000$ g m^{-3}, this corresponds to $Q = 2.0\times10^5$ W m^{-3} when heating is ON.

In time, the heating was applied as a train of rectangular pulses: after an initial delay of 10 s, we imposed n_{pulses} identical pulses of duration $\tau_{\text{pulse}} = 300$ s, separated by a period $T_{\text{pulse}} = 2300$ s (that is, 300 s ON followed by 2000 s OFF). During the ON intervals, the volumetric source Q was applied uniformly in the liquid; during the OFF intervals, Q was set to zero. No temperature boundary condition was imposed at the sensor tip; its temperature evolution arises solely from the imposed SAR in the liquid, thermal diffusion and heat losses to the ambient reservoir at $T_0 = 25$ °C.

5 SLP COMSOL-simulated values

As mentioned in the main text, numerical simulations were carried out to illustrate the behaviour of the PAM and ISM approaches in a controlled, physically realistic scenario. Fig. 6 shows the corresponding SLP values extracted from the COMSOL data, highlighting that the PAM yields higher SLP values than the ISM, in agreement with the experimental results.

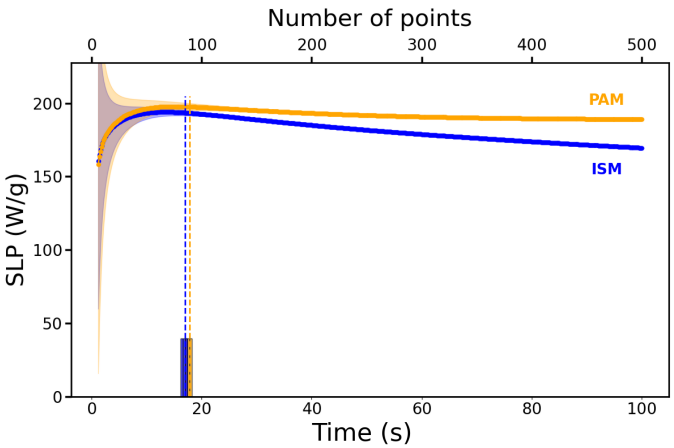

Fig. 6 SLP values obtained using both the PAM (orange) and ISM (blue) approaches as a function of the time interval considered for the linear fit, using the COMSOL-simulated data. Shaded regions represent the uncertainties associated with each method. The histograms displayed at the bottom of the figure show the distribution of the linear ranges identified by the F-test ($F < F_{\text{crit}}$), while the vertical dotted lines indicate the average optimal time window determined from this criterion.

Notes and references

1 P. De La Presa, Y. Luengo, V. Velasco, M. Morales, M. Iglesias, S. Veintemillas-Verdaguer, P. Crespo and A. Hernando, *The Journal of Physical Chemistry C*, 2015, **119**, 11022–11030.